Draft version September 2, 2025
Typeset using LaTeX **twocolumn** style in AASTeX7.0.1

Impact of Infalling Dust on Exoplanet Spectra

Eonho Chang,[1,2] Dominic Samra,[3] Peter Gao,[4] and Phil Arras[5]

[1] *Graduate Interdisciplinary Program in Applied Mathematics, University of Arizona, Tucson, AZ 85721, USA*
[2] *Department of Astronomy and Steward Observatory, University of Arizona, Tucson, AZ 85721, USA*
[3] *Department of Astronomy and Astrophysics, University of Chicago, Chicago, IL 60637, USA*
[4] *Earth & Planets Laboratory, Carnegie Institution for Science, Washington, DC 20015, USA*
[5] *Department of Astronomy, University of Virginia, Charlottesville, VA 22904, USA*

ABSTRACT

Theory and observations show planets can be surrounded by dust sourced from debris disks. Such dust can be accreted by a planet, affecting cloud formation by supplying condensation nuclei and/or additional condensable material. In this work, we examine the impact of Mg_2SiO_4 infall on Hot Jupiter atmospheres and their transmission spectra. We combine the 1D radiative-convective-chemical equilibrium model PICASO with the aerosol microphysics model CARMA. For WASP-17b analogs, we find dust accretion rates $\gtrsim 10^{11}$ g/s to significantly alter both size and vertical distribution of dust. We also synthesize transmission spectra with PICASO, which show molecular absorption features reduced by $\sim$20$-$30% of their original size for high infall (10^{11} g/s), whereas nominal infall (10^{8} g/s) results in spectra nearly indistinguishable from the no infall case. We predict Hot Jupiters with distant debris disk to show muted transmission spectral features, although no system is currently known to host both a Hot Jupiter and a debrisk disk. Observations of such systems may help us discern a particular Hot Jupiter formation scenario.

1. INTRODUCTION

Dust is always present in planetary systems, from the earliest stages of planet formation to mature planets around main sequence stars. In the millimeter continuum, observations of young protoplanetary disks ($\sim$Myr) show that concentration of mm-size dust grains in the shape of rings or crescents is common (S. M. Andrews et al. 2018). Near-infrared scattered light observations also show μm-size dust grains probing the vertical extent of disks (G. Duchêne et al. 2024).

More evolved ($\sim$10 Myr) transition disks undergo dissipation of gas and dust, but not complete depletion. For instance, mm-observations of PDS 70 show a large inner cavity of dust where young planets orbit, contrasted by a prominent dust ring outside their orbit (M. Keppler et al. 2018) and dust in their circumplanetary disks (M. Benisty et al. 2021).

Even after the planet-forming disk has dissipated, dust persists in the debris disk phase ($\sim$0.1$-$1 Gyr). In our Solar system, micron-size dust particles scatter sunlight to produce the zodiacal light in the Earth's night sky (M. C. Wyatt 2008). Observational surveys of nearby stars suggest about 20% have a thousand times more dust in mass (O. Absil et al. 2013; S. Ertel et al. 2014, 2020).

In debris disks, planetesimals undergo collisional cascade to continuously supply micron-size grains until the larger body reservoir runs out (J. S. Dohnanyi 1969; M. C. Wyatt 2008). Thus produced micron-size dust particles drift inward due to the Poynting-Robertson (PR) drag. For micron size particles, the radial drift timescale by the PR drag is $\sim$Myr at 40 AU, significantly less than the age of a typical debris disk system (see A. Moro-Martın 2013, for a review).

In the inner solar system, the zodiacal dust accretion rate is about $\dot{M} \sim 10^7$ g/s. Based on exozodiacal dust surveys, we expect $\dot{M} \gtrsim 10^{10}$ g/s for about 20% of nearby stars. Orbital simulations show the details of accretion – infall rate, deposition depth, gas-solid split – change depending on planet mass, semimajor axis and strength of vertical mixing (P. Arras et al. 2022).

Several Hot Jupiter systems show spectral signatures (e.g. muted features) consistent with high altitude clouds (D. Grant et al. 2023; C. Helling et al. 2023; J. Inglis et al. 2024). One possible pathway is to bring in-situ cloud upward by enhanced vertical mixing (D. Powell et al. 2018). Another possible explanation is infalling dust that we focus on in this study. The idea of such dust being accreted in different planet and dust particle conditions is investigated by P. Arras et al. (2022). Earlier work by P. Lavvas & T. Koskinen (2017) con-

sidered high-altitude haze from ablated meteoroid, and its impact on transmission spectra of Hot Jupiter HD 189733 b. Similarly, recent studies by J. Mang et al. (2022) and J. Mang et al. (2024) examined the effect of external meteoritic dust and photochemical haze serving as cloud condensation nuclei on temperate giant planets. In this work, we extend these ideas to test whether influx of external dust can form high altitude clouds and consequently affect their transmission spectra.

2. METHODS

2.1. *PICASO*

PICASO is a one dimensional exoplanetary atmosphere code that calculates the pressure-temperature (PT) structure given input parameters for the star and the planet (C. P. McKay et al. 1989; J. J. Fortney et al. 2005; N. E. Batalha et al. 2019; S. Mukherjee et al. 2023). With a given initial guess for the PT profile, PICASO iterates through solutions until the radiative-convective-chemical equilibrium is reached. We verified the converged PT profiles to be physically consistent (smooth lapse rate, radiative-convective boundary above the initial guess, etc).

PICASO takes as input stellar effective temperature $T_{\rm eff,*}$, stellar surface gravity $\log_{10} g_*$, metallicity [M/H], and stellar radius R_*. Then interpolates from the pre-computed stellar spectrum grid to synthesize a spectrum that corresponds to the stellar parameters specified. For all the runs presented here, we use the high-resolution PHOENIX models (F. Allard et al. 2012). We also tried the Castelli-Kurucz grid (F. Castelli & R. L. Kurucz 2003) and found the two stellar grids result in slightly different PT profiles.

For the planet, we specify planet surface gravity g and planet effective temperature $T_{\rm eff}$. For initial guessing of the PT profile, we utilize the parametric model by T. Guillot (2010), specifying the equilibrium temperature $T_{\rm eq}$ in addition to $T_{\rm eff}$. These temperatures are related in such a way that: $T_{\rm eff}^4 = T_{\rm eq}^4 + T_{\rm int}^4$ (see J. J. Fortney 2018, for a review), where $T_{\rm eq} \gg T_{\rm int}$ for highly irradiated planets like Hot Jupiters.

PICASO can take in the correlated-K (CK) table values for gas opacities. We use the high-resolution CK coefficients computed by R. Lupu et al. (2021).

In principle, for a tidally locked planet there are several longitudes (e.g. morning and evening limbs, substellar and antistellar points) that can have different PT profiles. Dust accretion is efficient for low inclinations, $\lesssim 10°$, but it remains unclear precisely where the infalling dust would concentrate in the atmosphere (P. Arras et al. 2022). For this initial study, we do not consider this effect and treat the planet atmosphere as homogeneous over different longitudes and latitudes in 1D.

2.2. *CARMA*

CARMA is a one-dimensional aerosol code that solves the discretized continuity equation, originally developed for Earth's atmosphere (R. P. Turco et al. 1979; O. B. Toon et al. 1979), and later adapted to exoplanet atmospheres (P. Gao et al. 2018; D. Powell et al. 2018). Given a PT profile, it can simulate how the dust cloud will form, taking into account particle transport processes – settling due to gravity and vertical mixing by eddy diffusion – as well as dust microphysics – nucleation, condensation, evaporation and coagulation. We run CARMA simulations to obtain a steady state size distribution and vertical number density profile.

To isolate the effect of nucleation and condensation, we use a reduced cloud condensate set, TiO_2 as a homogeneous nucleation species, and Mg_2SiO_4 as a heterogeneous species on top, and omit particle coagulation and fragmentation for this initial study. For Hot Jupiter clouds, coagulation is expected to be less important since the particles are already large whereas it becomes more important in hazes.

The infalling dust is prescribed as a mass flux at the upper boundary (10^{-6} bar). Based on the calculations by P. Arras et al. (2022), we split the dust influx into both gas and solid phases in 40/60, respectively. This allows for gas phase Mg_2SiO_4 to heterogeneously nucleate on either TiO_2 cores or solid phase Mg_2SiO_4 from infall. We resolve the dust size distribution from 10^{-4} to 3.3×10^3 micron with 75 bins, and the vertical distribution from 10^2 to 10^{-6} bar with 90 pressure levels.

2.3. *Setup*

We consider a nominal Hot Jupiter that is similar to WASP-17b. We take the stellar parameters for WASP-17 reported in the literature (taken from Exo.MAST), but vary planetary ones to explore the parameter space. Specifically, we choose two different distances away from the star, 0.149 AU and 0.051 AU, to produce equilibrium temperatures of $T_{\rm eq} = 1000$ K and $T_{\rm eq} = 1700$ K, respectively (the latter of which is physically consistent with WASP-17b). We also investigate two metallicity values, 1× Solar and 10× Solar. The CK tables used in this study exclude TiO, VO. The gas phase TiO VO would create an inversion layer in upper atmosphere, but only for ultra Hot Jupiters ($T_{\rm eq} \gtrsim 2400$ K), a temperature range not reached by our atmospheres at high altitudes. We verify that the computed atmosphere profiles don't show evidence of an inversion.

Letter	$T_{\rm eq}$ [K]	semimajor axis [AU]	[M/H]
a	1700	0.051	1.00
b	1700	0.051	0.00
c	1000	0.149	1.00

Table 1. Naming convention of PICASO models. Columns: (1) model letter, (2) planet equilibrium temperature, (3) planet semimajor axis, and (4) planet $\log_{10}$ metallicity with respect to Solar.

No.	$\dot{M}$ [$\dot{M}^{\rm ref}$]	a [μm]	K_{zz} [$K_{zz}^{\rm ref}$]	Notes
0	0	-	1	Control case
1	1	1	1	Nominal run
2	10^3	1	1	More flux
3	1	0.1	1	Smaller size
4	1	1	0.1	Nominal, less K_{zz}
5	1	1	K_{zz}@1 bar	Nominal, less K_{zz}
6	0	-	0.1	Control, less K_{zz}
7	0	-	K_{zz}@1 bar	Control, less K_{zz}
8	10^3	1	0.1	More flux, less K_{zz}
9	10^3	1	K_{zz}@1 bar	More flux, less K_{zz}

Table 2. Naming convention of CARMA runs. Columns: (1) simulation number, (2) dust infall rate, (3) infalling particle size, (4) vertical mixing coefficient, and (5) short description of each run setup. The reference accretion rate is $\dot{M}^{\rm ref} = 10^8$ g/s, and the reference vertical mixing coefficient profile $K_{zz}^{\rm ref}$ is taken from V. Parmentier et al. (2013).

Naming convention for our simulations is as follows: `[letter][number]`, where the lists of letters and numbers are given in Tables 1 and 2.

We first run PICASO for a particular setup and, using the computed PT profile, simulate the cloud distribution with CARMA. After the simulation has reached the quasi-steady state, we generate synthetic transmission spectra with the cloud distribution time-averaged over the last 10^8 seconds, a range that includes a few oscillation periods (e.g. see Fig. 2).

3. RESULTS

We mainly present results for model c as it shows the most dramatic differences between the no-infall and infall cases. Models a and b show similar trends, but the differences are less drastic. Fig. 1 shows PT profile for models a,b and c. Model c is convective for $10^1 - 10^2$ bar, and the rest of the atmosphere is radiative, almost tending to isothermal at 10^{-6} bar.

The CARMA simulations progress in three stages: 1) initial ramp up, 2) settling down, and 3) quasi-steady state with periodic oscillations. Fig. 2 shows a time series of CARMA simulation run on this PT profile with no infall (model c0). The initial ramp up lasts for $2-3 \times 10^7$ s, immediately followed by settling down. After that, the simulation reaches a quasi-steady state, exhibiting periodic behaviors in particle and vapor column densities until it is terminated at around 4.2×10^8 s. Although closer examination is required, we interpret these as a rain-cloud cycle (P. Gao & D. Powell, in prep).

Time evolution for the high infall run (model c2) is shown in Fig. 3. The general trend is similar to the no infall case, with an initial ramp up followed by settling down and quasi-steady cycles. Interestingly, the rise and fall of each peak appears more symmetric compared to the no infall case. Also, TiO_2 particle densities show larger oscillations relative to the maximum abundance. This may correspond to particles growing faster due to infall, leading to enhanced sedimentation and subsequent evaporation.

In addition to the TiO_2 core in blue and Mg_2SiO_4 outer shell in orange, the high infall case has another curve in red which corresponds to pure Mg_2SiO_4 particles. Pure Mg_2SiO_4 particles exist now due to infalling solid acting as condensation sites. The density of pure Mg_2SiO_4 particles reaches its maximum value very quickly, $<10^7$ s, and remains stable until the end of simulation. Similar behavior is seen in vapor mass column density, indicating dominant contribution from the continuous infall, which has both gas and solid components.

Fig. 4 shows snapshots of dust distributions at the end of each simulation. Looking at the no infall case, we see a cloud deck forming between 10^1 and 10^2 bar, and the number density decreases upward like a powerlaw. At $\sim 10^{-3}$ bar, (dotted line), differential size distribution shows Mg_2SiO_4 growing on top of TiO_2 core, with characteristic size up to ~ 10 micron.

In the case of nominal infall (10^8 g/s), the vertical dust distribution is nearly identical to the no infall case. The peak near 1 micron in the size distribution comes from the input value at 1 micron. But the peak value lies below the in-situ Mg_2SiO_4 cloud. Interestingly, Mg_2SiO_4 grows on top of smaller TiO_2 cores compared to the no-infall case, where the tail of the size distribution now extends down to $\sim 10^{-3}$ microns whereas the tail goes down to $\sim 10^{-1}$ microns in the no-infall case.

In the high infall case (10^{11} g/s), a distinct high-altitude cloud layer appears. The vertical distribution shows a secondary cloud population at higher altitudes, $\sim 10^{-3}$ bar. The peak in the size distribution from infall extends above the in-situ cloud. TiO_2 cores are concentrated at smaller sizes ($\lesssim 10^{-3}$ micron). The size distribution also shows relative depletion of particles between 10^{-3} and 10^{-2} microns compared to the two other runs. This may be owing to the fact that now TiO_2 cores must

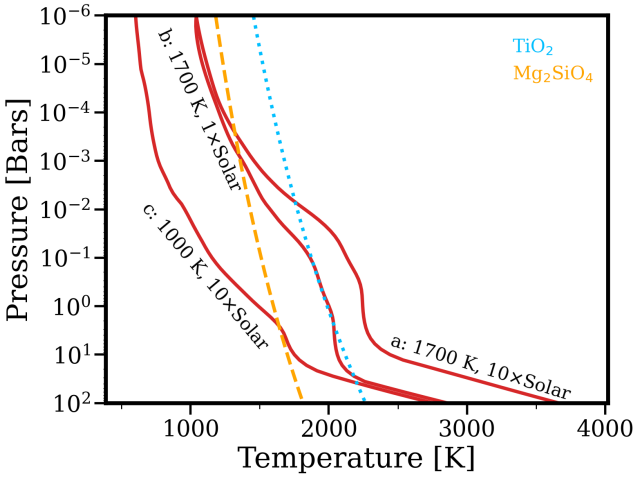

Figure 1. Vertical structure for different models computed with PICASO. PT profile (red solid), Mg_2SiO_4 condensation curve (orange dashed) and TiO_2 condensation curve (blue dotted) are shown.

compete with infalling Mg_2SiO_4 seeds as condensation nuclei.

Fig. 5 show mock transmission spectra representative of the quasi-steady state for the three different cases. The nominal infall rate case is pretty much indistinguishable from the no infall case, whereas the high infall rate case stands out a lot. The spectral features are muted, as much as 20−30% of original size of the feature (e.g. CO_2 at 4.5 micron). It also shows the silicate bump around 10 micron.

Shorter wavelengths $\lesssim$ 1 micron is less reliable, possibly due to numerical artifacts or Mie resonance from the monodisperse infall size.

The stark contrast between models c1 and c2 suggest a threshold in infall rate that can significantly affect the dust distribution and transmission spectra. This behavior is also seen in the models a[0-2] and b[0-2].

4. DISCUSSION

For the first time, we examined the effect of physically motivated infalling dust on cloud distribution in exoplanet atmospheres and their spectra. Our infall scenarios use values consistent with theoretical and observational estimates. Building on previous studies that examined the impact of dust from meteoroid ablation (P. Lavvas & T. Koskinen 2017; J. Mang et al. 2022, 2024) and zodiacal dust infall calculations (P. Arras et al. 2022), we explicitly model how infalling dust modifies cloud distribution and their observational features in Hot Jupiters.

Our models show that nominal infall rates ($\dot{M} = 10^8$ g/s) have little effect. With high enough flux ($\dot{M} = 10^{11}$ g/s), however, we show it is possible to significantly alter

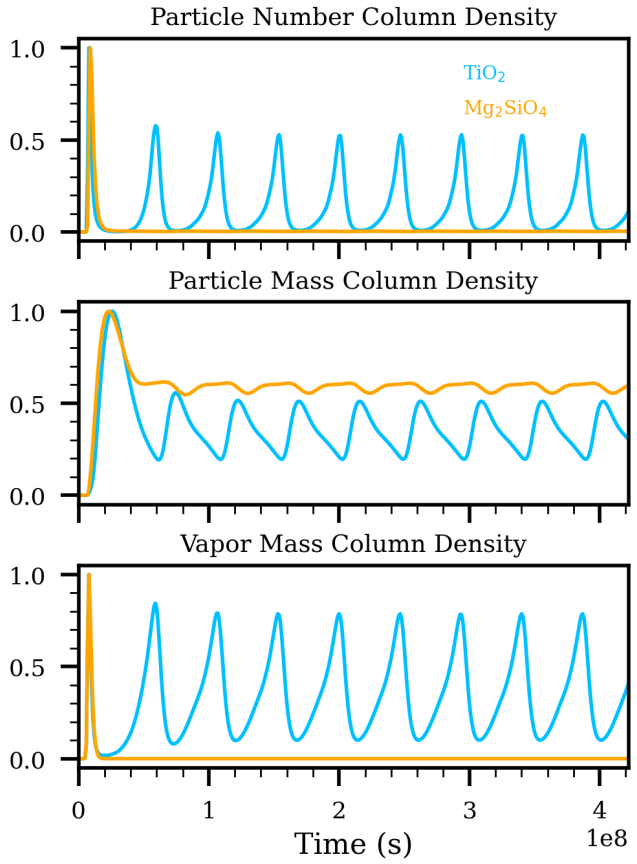

Figure 2. Time series of CARMA simulation for no infall (model c0). Each quantity is normalized such that maximum is 1. Blue is TiO_2 core, orange is Mg_2SiO_4 outer shell on top of TiO_2 core.

both the dust distribution (Fig. 4) and the transmission spectrum (Fig. 5) of a Hot Jupiter. Our results suggest Hot Jupiters in dust rich systems will have muted spectral features in their transmission spectra.

To date, no known systems host both transiting Hot Jupiters and debris disks (in the near-infrared). This idea can be tested with observations. Our results can serve as a guide for observational studies to follow up and test this hypothesis by searching for these systems.

Observations of such systems would favor a particular pathway for Hot Jupiter formation. Two main hypotheses are known: migration within disk during formation, and high-eccentricity migration after disk dissipation (see J. J. Fortney et al. 2021, for a review). The infalling dust hypothesis seems less compatible with high-eccentricity migration, as excitation and circulization of the planet's orbit may disrupt the debris disk sourcing micron size dust via chaotic dynamical interactions. Therefore, formation of Hot Jupiters with far out debris disk would be aligned with the more quiescent disk migration scenario.

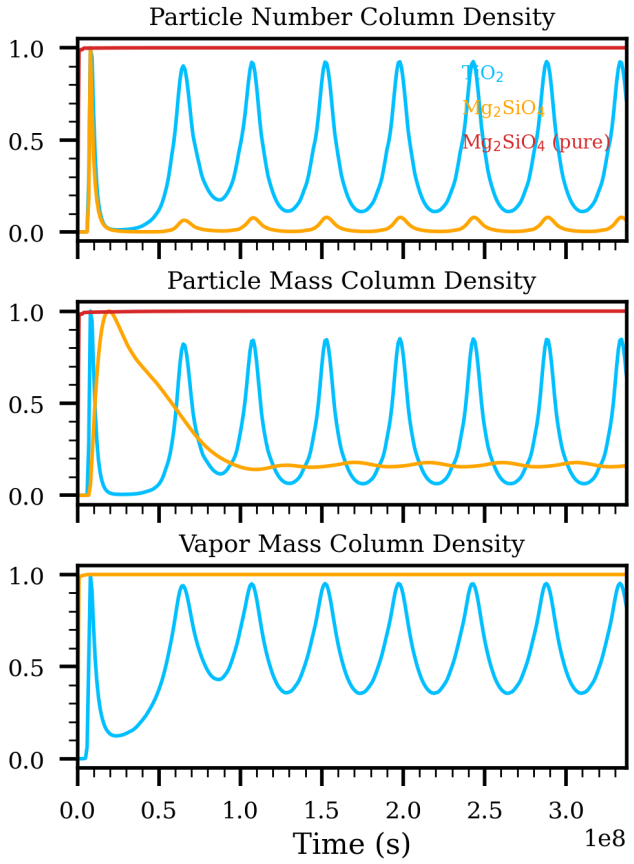

Figure 3. Similar to Fig. 2 but for high infall (model c2). Red curve denotes pure Mg_2SiO_4.

Our framework is general, and may also apply to young planets far away from the star (e.g. PDS 70 b,c), which may be shrouded by an envelop or disk of material that provide a source of external dust. Preliminary results suggest that for reasonable values of accretion rates the emission spectra for such planets can also be altered significantly. Specifically, for dust accretion rates $\dot{M} \gtrsim 10^{-10}\,M_{\rm J}/{\rm yr}$ ($\approx 6\times10^{12}$ g/s), we find opacity of the infall dust clouds can heat up the upper atmosphere ($P \lesssim 1$ bar) by 500−1000 K, and redden the emission spectra to appear more like a blackbody continuum.

ACKNOWLEDGEMENTS

The authors thank Natasha Batalha, Andrew Youdin and Yifan Zhou for helpful discussions. The CARMA simulations were run on the vger HPC cluster at Carnegie EPL. This work originated from a project of the Summer Program in Astrophysics 2025 held at the University of Virginia, and funded by the Center for Global Inquiry and Innovation, the National Science Foundation (Grant 2452494), the National Radio Astronomy Observatory (NRAO), the Kavli Foundation and the Heising-Simons Foundation.

REFERENCES

Absil, O., Defrère, D., Foresto, V. C. d., et al. 2013, Astronomy & Astrophysics, 555, A104, doi: 10.1051/0004-6361/201321673

Allard, F., Homeier, D., & Freytag, B. 2012, Philosophical Transactions of the Royal Society A: Mathematical, Physical and Engineering Sciences, 370, 2765, doi: 10.1098/rsta.2011.0269

Andrews, S. M., Huang, J., Pérez, L. M., et al. 2018, The Astrophysical Journal Letters, 869, L41, doi: 10.3847/2041-8213/aaf741

Arras, P., Wilson, M., Pryal, M., & Baker, J. 2022, The Astrophysical Journal, 932, 90, doi: 10.3847/1538-4357/ac625e

Batalha, N. E., Marley, M. S., Lewis, N. K., & Fortney, J. J. 2019, The Astrophysical Journal, 878, 70, doi: 10.3847/1538-4357/ab1b51

Benisty, M., Bae, J., Facchini, S., et al. 2021, The Astrophysical Journal Letters, 916, L2, doi: 10.3847/2041-8213/ac0f83

Castelli, F., & Kurucz, R. L. 2003, New Grids of ATLAS9 Model Atmospheres, eprint: arXiv:astro-ph/0405087: arXiv, doi: 10.48550/arXiv.astro-ph/0405087

Dohnanyi, J. S. 1969, Journal of Geophysical Research (1896-1977), 74, 2531, doi: 10.1029/JB074i010p02531

Duchêne, G., Ménard, F., Stapelfeldt, K. R., et al. 2024, The Astronomical Journal, 167, 77, doi: 10.3847/1538-3881/acf9a7

Ertel, S., Absil, O., Defrère, D., et al. 2014, Astronomy & Astrophysics, 570, A128, doi: 10.1051/0004-6361/201424438

Ertel, S., Defrère, D., Hinz, P., et al. 2020, The Astronomical Journal, 159, 177, doi: 10.3847/1538-3881/ab7817

Fortney, J. J. 2018, Modeling Exoplanetary Atmospheres: An Overview, arXiv, doi: 10.48550/arXiv.1804.08149

Fortney, J. J., Dawson, R. I., & Komacek, T. D. 2021, Journal of Geophysical Research: Planets, 126, e2020JE006629, doi: 10.1029/2020JE006629

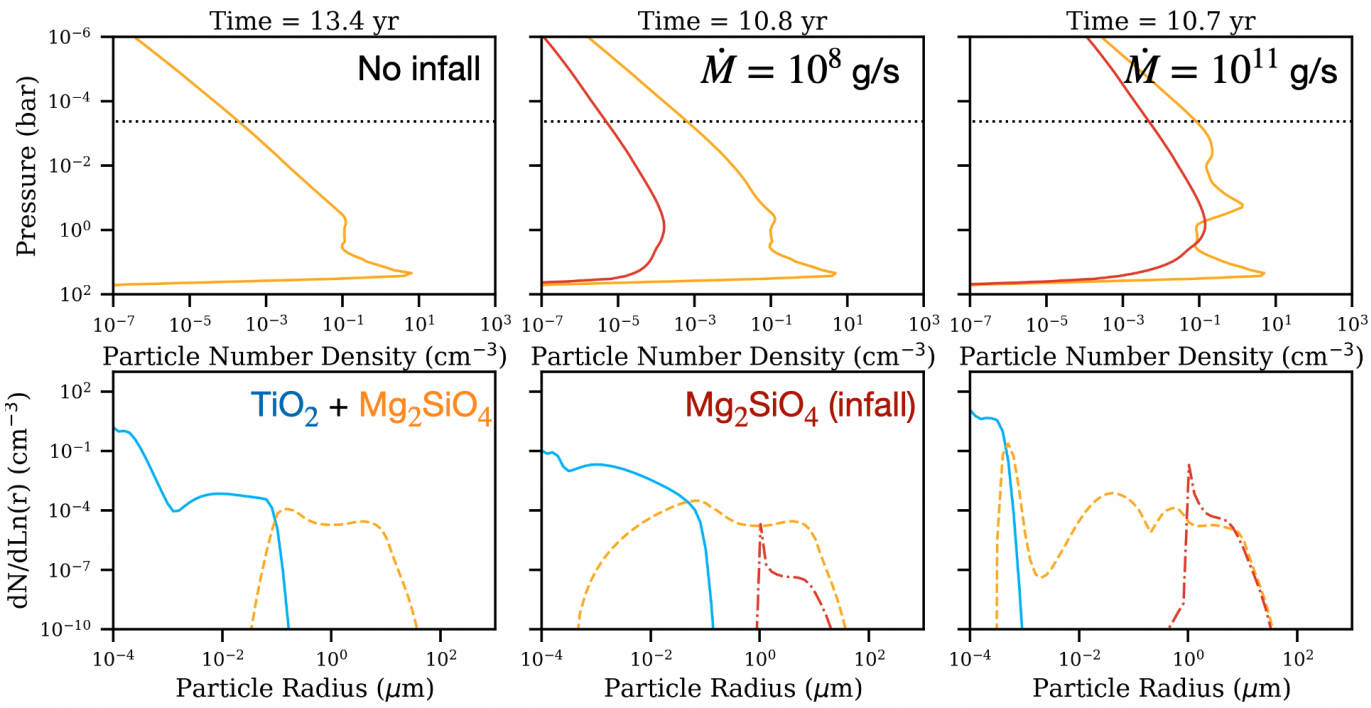

Figure 4. CARMA simulation snapshots for three different infall rates (different columns). Top: vertical distribution of dust in number density. Bottom: size distribution of dust.

Fortney, J. J., Marley, M. S., Lodders, K., Saumon, D., & Freedman, R. 2005, The Astrophysical Journal, 627, L69, doi: 10.1086/431952

Gao, P., Marley, M. S., & Ackerman, A. S. 2018, The Astrophysical Journal, 855, 86, doi: 10.3847/1538-4357/aab0a1

Grant, D., Lewis, N. K., Wakeford, H. R., et al. 2023, The Astrophysical Journal Letters, 956, L32, doi: 10.3847/2041-8213/acfc3b

Guillot, T. 2010, Astronomy & Astrophysics, 520, A27, doi: 10.1051/0004-6361/200913396

Helling, C., Samra, D., Lewis, D., et al. 2023, Astronomy & Astrophysics, 671, A122, doi: 10.1051/0004-6361/202243956

Inglis, J., Batalha, N. E., Lewis, N. K., et al. 2024, The Astrophysical Journal Letters, 973, L41, doi: 10.3847/2041-8213/ad725e

Keppler, M., Benisty, M., Müller, A., et al. 2018, Astronomy & Astrophysics, 617, A44, doi: 10.1051/0004-6361/201832957

Lavvas, P., & Koskinen, T. 2017, The Astrophysical Journal, 847, 32, doi: 10.3847/1538-4357/aa88ce

Lupu, R., Freedman, R., Gharib-Nezhad, E., Visscher, C., & Molliere, P. 2021, Correlated k coefficients for H2-He atmospheres; 196 spectral windows and 1460 pressure-temperature points, Zenodo. https://zenodo.org/records/5590989

Mang, J., Gao, P., Hood, C. E., et al. 2022, The Astrophysical Journal, 927, 184, doi: 10.3847/1538-4357/ac51d3

Mang, J., Morley, C. V., Robinson, T. D., & Gao, P. 2024, The Astrophysical Journal, 974, 190, doi: 10.3847/1538-4357/ad6c4c

McKay, C. P., Pollack, J. B., & Courtin, R. 1989, Icarus, 80, 23, doi: 10.1016/0019-1035(89)90160-7

Moro-Martın, A. 2013, in Planets, Stars and Stellar Systems (Springer, Dordrecht), 431–487, doi: 10.1007/978-94-007-5606-9_9

Mukherjee, S., Batalha, N. E., Fortney, J. J., & Marley, M. S. 2023, The Astrophysical Journal, 942, 71, doi: 10.3847/1538-4357/ac9f48

Parmentier, V., Showman, A. P., & Lian, Y. 2013, Astronomy & Astrophysics, 558, A91, doi: 10.1051/0004-6361/201321132

Powell, D., Zhang, X., Gao, P., & Parmentier, V. 2018, The Astrophysical Journal, 860, 18, doi: 10.3847/1538-4357/aac215

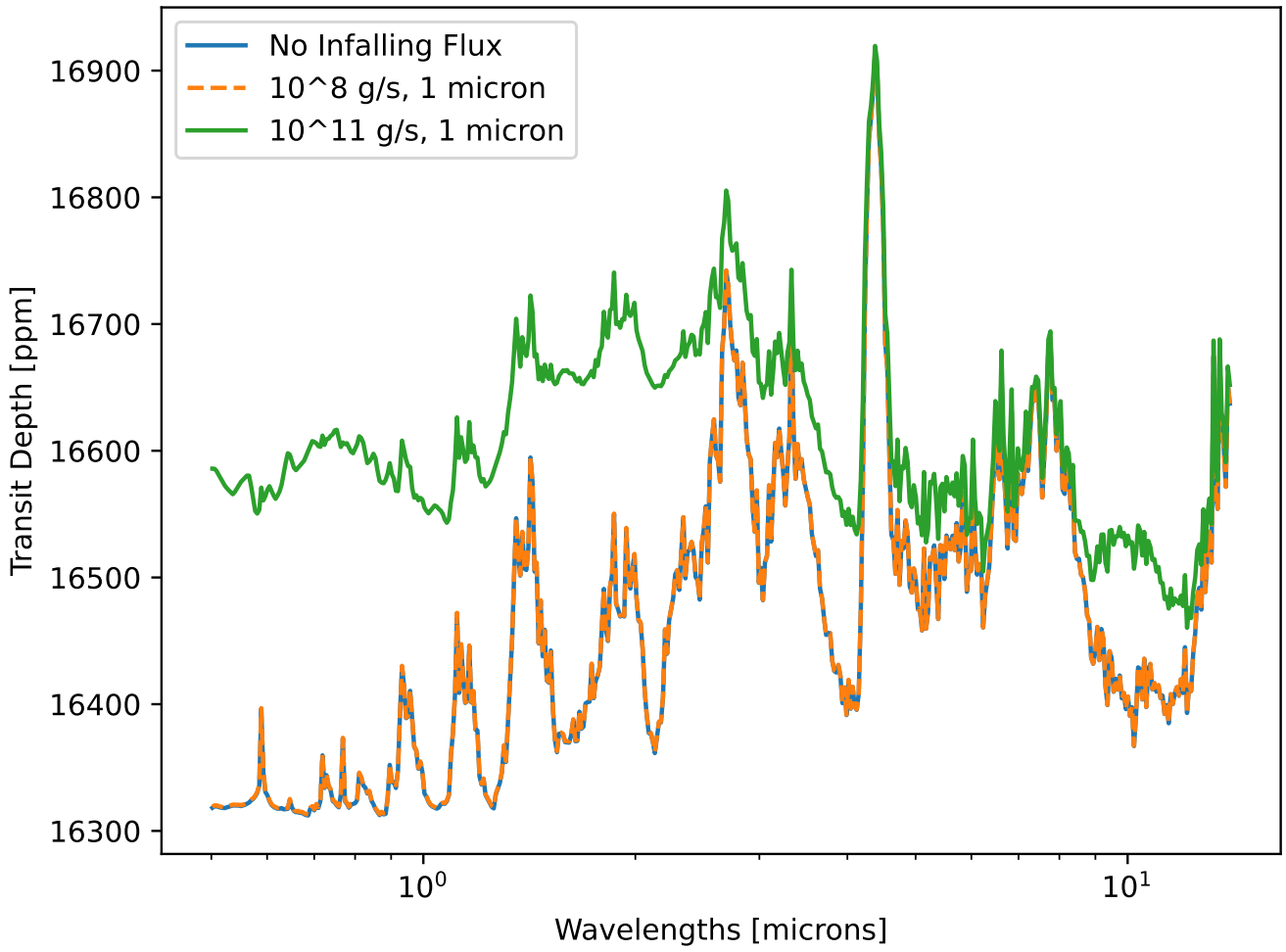

Figure 5. Transmission spectra for three different dust infall rates.

Toon, O. B., Turco, R. P., Hamill, P., Kiang, C. S., & Whitten, R. C. 1979, https://journals.ametsoc.org/view/journals/atsc/36/4/1520-0469_1979_036_0718_aodmda_2_0_co_2.xml

Turco, R. P., Hamill, P., Toon, O. B., Whitten, R. C., & Kiang, C. S. 1979, https://journals.ametsoc.org/view/journals/atsc/36/4/1520-0469_1979_036_0699_aodmda_2_0_co_2.xml

Wyatt, M. C. 2008, Annual Review of Astronomy and Astrophysics, 46, 339, doi: 10.1146/annurev.astro.45.051806.110525